

Outline of climate and oceanographic conditions in the Indian Ocean: an update to mid-2016

Francis MARSAC¹ & Hervé DEMARCQ²
IRD
UMR 248 MARBEC
Sète, France

Abstract

Several descriptors of the ocean climate conditions are examined to depict the inter-annual trend and to track major changes that may affect the large pelagic ecosystem. The environmental series were updated to July 2016 and September 2016 depending on the variables. The main feature is the development of a strong positive Indian Ocean Dipole during the second semester of 2015. This dipole has coincided with the ENSO warm phase, with development of an El Niño event in the Pacific Ocean. The anomalies associated to the positive dipole were warmer sea surface temperature over most of the Indian Ocean, a deep thermocline ridge in the West Indian Ocean through November 2015 - May 2016 and a depleted primary productivity in the South Arabian Sea and in the Somali basin. The dipole turned into a negative phase in January 2016, reached its mature condition in May 2016 and is predicted to continue through the boreal fall. As expected during a positive dipole phase, the primary productivity has been reduced in the western region of the IO from July 2015 to February 2016 and has returned to a more productive phase since May 2016. The vertical current shear in the upper water column (4 to 145m) exhibits two distinct patterns along with the dipole situation, with weaker shear during positive dipoles and stronger shear during negative dipoles. Because of this pattern, it is suggested that further consideration be given to use the vertical shear current as an additional environmental covariate in bigeye CPUE standardization.

1 Data access and preparation

1.1 Climate indices

The Southern Oscillation Index (SOI) is documented in many websites. A comprehensive analysis of trends of a number of climate and oceanic variables, and climate updates at a global scale are found in the Climate Diagnostics Bulletin of the CPC/NOAA at the following URL http://www.cpc.noaa.gov/products/analysis_monitoring/bulletin/.

The Indian Oscillation Index (IOI) was introduced by Marsac and Le Blanc (1998). Similarly to the SOI, this index is the difference of standardized anomalies of the sea level pressure (SLP) in two distant sites characterized by a dipole-like pattern, namely Darwin and Mahé (Seychelles) for the IOI. The SLP data were provided by the Climate Centre of the Seychelles National Meteorological Services National. The series is updated monthly (until September 2016) and the whole series, starting in 1951, is available with the author.

1.2 Sea surface temperature and thermocline depth

The Extended Reconstructed Sea Surface Temperature (ERSST) dataset is a global monthly sea surface temperature dataset derived from the International Comprehensive Ocean–Atmosphere

¹ Email : francis.marsac@ird.fr

² Email : herve.demarcq@ird.fr

Dataset (ICOADS). It is produced on a $2^\circ \times 2^\circ$ grid with spatial completeness enhanced using statistical methods. ERSST is suitable for long-term global and basin-wide studies, and smoothed local and short-term variations are used in the dataset (Huang et al, 2015). The monthly anomalies were calculated from a climatology established by the author over the period 1971-2000.

The Dipole Mode Index (DMI), that quantifies the Indian Ocean Dipole (Saji et al, 1999), is obtained by subtracting the SST anomalies between the West and East Indian Ocean. The west box is $50^\circ\text{E}/10^\circ\text{N}-10^\circ\text{S}$ and the east box is $90^\circ\text{E}-110^\circ\text{E}/0^\circ-10^\circ\text{S}$. The ERSST dataset was used to compute the DMI.

The study of the variability patterns and the regional environmental assessments was carried out with the outputs of the NOAA/NCEP Global Ocean Data Assimilation System (GODAS), which provide monthly fields of temperature, salinity, vertical velocity and current for 40 depth levels (5 to 4500 m), along a 1° longitude/ 0.33° latitude grid globally. Here, we use the depth of the 20°C isothermal depth (Z20) as a proxy for the thermocline. Z20 is obtained by interpolation between consecutive depth levels. We also computed the vertical current shear between two depth levels of the GODAS model (5 and 145 m). The shear between two levels z_1 and z_2 is obtained by:

$$S = \text{Log}(W / \Delta z)$$

With u : zonal component of the current

v : meridional component of the current

Δu , Δv and Δz , difference of u and v between the 2 levels (5 and 145 m)

$$U = (\Delta u / \Delta z)^2 \quad \text{and} \quad V = (\Delta v / \Delta z)^2$$

$$W = \text{SquareRoot}(U+V) \times \Delta z$$

For all variables, the monthly anomalies were calculated from a climatology established by the author over the period 1980-2005.

1.3 Sea surface chlorophyll

The chlorophyll product of the SeaWifs (1997-2002) and Modis (2002 to present) sensors were used to study the trends in sea surface chlorophyll (SSC). The original dataset is the Level-3 monthly composite at a 9-km resolution. In order to combine the analyses with SST and Z20, we re-gridded the level-3 dataset at the same spatial resolution as the NCEP-GODAS model output ($1^\circ\text{Lon}/0.33^\circ\text{Lat}$). The monthly anomalies were calculated from a climatology established by the author over the period 2003-2008. The transition between SeaWifs and Modis series was done by averaging values of both sensors over a common period of 6 months (July to December 2002).

2 Results

2.1 Development of a strong El Niño in 2015/2016

The El Niño event 2015-2016 has been among the strongest ever recorded. Monthly values of the SOI were at their minimum in January and February 2016 (below -2) marking an intense event (Fig. 1). El Niño started to develop in March-April 2015, reached mature conditions during the 4th quarter of 2015 and vanished in May 2016. During El Niño, rainfall became anomalously high in the subtropical regions of Southern America and over the south of the USA and north of Mexico. By contrast, the northern region of South America (including the Amazonian forest) was hit by a severe drought. On the other side of the Pacific Ocean, Indonesia was anomalously dry (causing many forest fires), as well as in the West Indian Ocean, such as the horn of Africa and Southern Africa.

A major characteristic of the 2015-2016 Niño is the location of the warm anomaly. Whereas the positive SST anomaly peaked in the East Pacific during the intense of 1982-83 and 1997-98 El Niño events, it was mostly located in the Central Pacific ocean in 2015-16. The chain of events leading to the El Niño 2015-2016 was investigated by Aaron et al (2016). Westerly wind bursts in spring 2014 were thought to trigger an El Niño for 2014-2015. However, this event failed to kick in because of

strong easterly wind burst occurring in summer. The progression of the warm anomaly was therefore stopped in the Central Pacific Ocean, and the poleward discharge of heat content did not happen. The existence of this elevated heat content at the equator (Fig. 2) contributed to push the 2015-2016 El Niño to extreme magnitude.

The 2015-2016 El Niño happened after a period of 27 consecutive months of ENSO-neutral conditions (Nov 2012-Jan 2015). The SOI fluctuations about the baseline during this period (Fig. 1) notably in 2013, were not sustained at sufficient levels over time to be considered as significant events.

According to the Climate Diagnostic Bulletin of the NOAA, the combined ocean and atmosphere system during September 2016 reflects ENSO-neutral conditions. Model ensemble predictions and recent cooling of the Niño-3.4 regions favour the formation of a weak La Niña (~70% chance) during the boreal fall and that such conditions persist over the coming winter (55% chance). The La Niña type conditions are reflected by negative temperature anomalies of the Niño 3-4 region (5°N-5°S / 120°W-170°W) as shown in Figure 3.

2.2 Indian Ocean Dipole mode

Since 2007, the IOD index has been mostly in the positive area, with significantly strong dipoles (i.e. warm episodes in the WIO) in Sept 2006-Jan 2007, Jul-Dec 2012 and Jul-Nov 2015. Such dominance of positive dipoles coincides with a similar trend of the IOI becoming mostly negative (also associated to a warmer WIO) (Fig. 4). Negative IOD events such as Jul-Oct 200 and Aug-Oct 2010 occurred with a lesser magnitude and during shorter period of time than positive events. The most recent negative dipole has reached its mature condition in May 2016 and is still ongoing. The magnitude of this event is quite strong, with peak value of -0.8 (in Jul 2016) and 5-month smoothed values below -0.4 since March 2016 (Fig. 4). The IOI has shifted to high positive values (reflecting a colder than normal WIO since June 2016, with a peak to Sept 2016 (last available observation) at +2.3.

The dipole forecast analysis performed by the Australian Bureau of Meteorology predicts return to normal dipole conditions at the beginning of 2017, and a persistence into this neutral phase throughout the first semester of 2017 (Fig. 5).

2.3 Long-term SST trend

Using the ERSST v4 dataset, we computed the average monthly SST anomalies over the whole Indian Ocean (40°E-100°E / 20°S-20°N) for 1995-2016. An overall increasing trend can be noticed over this period, although anomalies were fluctuating without trend during 2003-2008 (Fig. 6a). The detrended series underlines the warmest events, at the turn of 1997-98, early 2010, and most of the year 2015, with SST ranging from 0.4 to 0.6°C above the long-term mean (Fig. 6b). Strong negative SST anomalies occurred in 1996, 2008, 2011, 2013 and 2016.

2.4 Basin-scale patterns

SST, Thermocline depth and Sea surface chlorophyll (SSC)

A full set of monthly maps over the Indian Ocean for 2015-2016 is provided in the power point presentation of this paper. Here, we provide only a limited set showing the first month of each quarter, from January 2015 to July 2016 (Fig. 7a, 7b).

SST anomalies in Jan and Feb 2015 were negative off Somalia, whereas a warm pool was present in the SE tropical Indian Ocean. During the same period, thermocline was lifted 30-50 m upwards off Somalia, in the Seychelles area (south equatorial counter-current). Deep thermocline was located at the northern tip of Madagascar, South of Reunion and in the Central IO. SSC anomalies were highly positive in the Arabian Sea and along the Somalian coast. Such positive SSC anomalies coincided most of the time with shallow thermocline.

From April to June 2015, the warm pool expanded in a westward direction and anomalies above 1.5°C started to appear along 10°S. A large cyclonic ring which started to develop in February at

17°S/60-70°E gradually moved to the west and reached its greatest magnitude during that quarter. Thermocline was lifted 60 to 80 m upwards in the core of the ring. SSC remain normal in April (that is low values). High SSC anomalies appeared along the Somalian coast from the very start of the southwest monsoon.

From July to September 2015, the warming spread over the whole Indian Ocean. In July, SST became cooler off Sumatra but this remained moderate (anomaly of -0.5 to -1°C) whereas positive SST anomalies the WIO were above 1°C. As for thermocline depth, a deep thermocline ridge started to develop along 10°S, moving in a westward direction (deepening of 30-40 m). The cyclonic ridge (with shallow thermocline) continued to move towards Madagascar, with decreasing intensity. SSC anomalies remained positive in July off Somalia, then turned into a negative state west of 60°E in the equatorial region, and in several of the visible areas of the Arabian Sea (observations in this region are limited by the cloud cover)

During the last quarter 2015, the warming intensified in the West (1° to 2°C above normal). By contrast, the cooling off Sumatra did not persist after November. The deep thermocline ridge continued to expand to the west, whereas the cyclonic ring crashed on Madagascar and decayed in December. SSC anomalies were negative, denoting a depleted productivity along the Somalia coast and off Kenya. Negative SSC anomalies also developed in Maldives, Chagos and south of Seychelles.

From January to March 2016, warm SST anomalies persisted over the whole IO. The deep thermocline ridge reached its full magnitude (deepening of 50-60m) and expansion (5° to 10°S), which is a typical feature of El Niño/Positive dipole event. By contrast, shallower thermocline (lifted by 20 to 30m) developed in the Eastern IO (5°-11°S, 80°-100°E). SSC anomalies remained negative in the westernmost areas of the WIO, indicating continuation of a depleted chlorophyll situation in the epipelagic environment.

During the second quarter 2016, warm SST anomalies started to decline along the African coast, with a transition to cold anomalies off Somalia in June, indicating the onset of a strong upwelling. The deep thermocline ridge reached Tanzania in April where it persisted until June. It vanished elsewhere in May and June. Thermocline shoaling was observed off Somalia. With such transition to cooler conditions and shallower thermocline, the primary production was enhanced in the WIO. The SST, thermocline and SSC trend reflecting negative dipole conditions continued in July 2016.

Vertical current shear

The vertical current shear displays two distinct patterns depending on the dipole situation. During positive dipoles, the shear tends to be lesser than during negative dipoles. Shear anomalies are negative in most of the regions of the Indian Ocean at the peak phase of the positive dipole (Fig. 8). This is quite clear in March 1982, May 1994 and September 2015. In January 1998, weak shear prevailed in the WIO whereas strong shear occurred along a latitudinal band 6°S-10°S east of 70°E. In November 2006, strong shear was restricted to the Seychelles area (3°S-7°S, 45°-70°E) and South Java, whereas it was weak in the rest of the equatorial region. In August 2008, the only strong shear occurred in the band 0°-3°S, east of 80°E.

Positive shear anomalies are dominant along the equator at the peak of the negative dipole phase (Fig. 9). However, the pattern is not as clear and extensive as it is during positive dipole events with negative shear anomalies.

2.5 Regional analyses

The regional outlook is performed for 5 different sub-areas of the Indian Ocean (Fig. 10). As such analysis is a follow-up, on a yearly basis, of previous outlooks (Marsac, 2011 to 2015), we shall not go into details for the whole series which starts in 1998.

The sea surface chlorophyll (SSC) concentration by sub-area is presented in Fig. 11. Somalia (SOM) and Mozambique Channel (MOZ) are the most productive regions, with SSC ranging 0.30 to 0.54

mg.m⁻³. The major anomaly in the series is the exceptionally high chlorophyll content in Somalia, in 2002-2005. Another group, Maldives (MAL) and the West equatorial region (WEQ), displays comparable values (0.11 to 0.22 mg.m⁻³). The SSC in the East tropical region does not fluctuate much and remain at a low average level (0.08 to 0.12 mg.m⁻³). The SSC has been increasing (with fluctuations) in SOM since 2012, as well as in MAL and WEQ. The provisional 2016 SSC is a record for MOZ (0.44 mg.m⁻³, 15% above average), 10% above average for SOM and 17% above average for WEQ. Because of the long declining trend of SSC in MAL since 2001, and despite the slight increase since 2012, the 2016 SSC is 9% below average.

Summaries of SST, Z20 and chlorophyll are given for each area, considering some specific months or seasons.

Somalia (June-September, Fig. 12): the SST and chlorophyll anomalies fluctuate in phase, with cold (warm) year corresponding to high (low) primary productivity. Along with warmer SST in 2015, the SSC was low (12% below average) and the situation is reversing in 2016 in line with the negative dipole.

Mozambique Channel (January-July, Fig. 13): overall, SST and SSC fluctuate with opposite anomalies. Not fitting with this model, relatively high SSC anomalies were observed in 2016, along with warm SST. This result is due to averaging values over a contrasted 6-month period. In details, the positive SST anomalies occurred during Jan-March (a consequence of the positive dipole) when SSC was slightly below normal. Positive SSC anomalies developed in April when SST anomalies were either normal or slightly below average.

West equatorial region (December-February, Fig. 14): the 2015/2016 cumulated SST anomaly (+2.6°C) reached the same magnitude as during the 1997/1998 positive dipole/El Niño event. The thermocline deepened during 2015/2016 (by 8m) however far less than the deepening seen in 1997/1998 (30m). The response in chlorophyll was very weak decline (-5%) compared to 1997/1998 or 2011/2012.

Maldives (January-August, Fig. 15): Positive SST anomalies have prevailed in the Maldives since 1997. The highest cumulated SST anomalies happened in 1998 (+5.2°C) during an positive dipole, and in 2016 (+4°C) before the negative dipole starts to develop. Thermocline depth was normal, at the mean level of the series. Two regimes characterize the chlorophyll anomalies around Maldives: positive phase for 1998-2002 and negative phase during 2007-2016 (with an exception in 2015).

East tropical area (July_{y-1} – June_y, Fig. 16): the 12 month period from mid-2015 to mid-2016 has been the warmest ever recorded in this region, after a steady increase of SST anomalies since 2012. The SSC response is a depleted state for the same period of time. Chlorophyll anomalies exhibit two regimes, dominated by positive anomalies for 1998-2000 (in relation to La Niña), and by negative anomalies for 2008-2016, with the exception of 2011 in relation with a Niña event.

3 Discussion on catchability for purse seine and longline fisheries in relation to the dipole event

A strong positive dipole developed in the Indian Ocean during the second semester of 2015. This dipole has coincided with the ENSO warm phase, with development of an El Niño event in the Pacific Ocean. The SST anomaly field became highly positive over most of the tropical IO culminating during the dipole and persisting until April 2016, much after the decay of the IOD. The deep thermocline ridge at 10°S which normally develops along with the positive dipole in the WIO started to develop in November 2015, culminated in February 2016 and vanished in May 2016. As expected during positive dipole, the primary productivity has been reduced in the western region of the IO from July 2015 to February 2016.

Thermocline depth is known to affect catchability in purse seine fisheries. Considering the free school fishing season (spanning December to February), very distinct situations were found in 2014-2015

and 2015-2016 as shown in Figure 17. During 2014-2015, yellowfin CPUEs were distributed over the shallow thermocline areas (negative anomalies, in dark green and blue in the figure) and average CPUEs were 7.9, 22.4 and 30.6 t/day for Dec 2014, Jan and Feb 2015 respectively. By contrast, CPUEs were reduced by 50% in 2015-2016 compared to the previous year (9.9, 11.1 and 14.6 t/day for Dec 2015, Jan and Feb 2016 respectively). One probable cause of such decline is the existence of a deep thermocline ridge in the fishing zone between 5°S-10°S that has deepened the tuna habitat and made tunas less available to the purse seiners. Reducing mortality of yellowfin spawners in one of their core zone may induce a beneficial effect for the stock biomass in 2016. It is likely that catchability for purse seiners would have been promoted in the East Indian Ocean as the thermocline was lifted by 40m in November-December off Sumatra. However, this anomaly was not as strong as the one in 1997-1998, when purse seiners left the WIO fishing grounds to operate in the East Indian Ocean.

The vertical current shear exhibits a pattern of relatively weak magnitude during positive dipoles, and stronger magnitude during negative dipole events. The vertical shear can influence the shape of the longline. Boggs (2012) observed that hook depths were shallower than those predicted from the catenary geometry especially in deep sets (> 300m) in areas with strong currents. Here, we present maps of vertical current shear estimated from two depth levels (5 and 145 m) produced by the NCEP GODAS ocean model. The two patterns associated to opposite dipole situations would be worth to be considered in longline CPUE standardization for bigeye, as this species is mostly concerned by deep sets. The current shear also exhibits some long-term trend. Taking the example of the East Indian Ocean (80°-100°E, 0°-15°S) which is a bigeye core fishing zone for Japanese longline fishery, the shear has been increasing from 1980 to the end of 1990s, then declined since the early 2000s. Such trend exists whatever the month selection. In Figure 18, we present shear time series at different seasons: low shear (Jan-Mar), maximum shear (Aug-Oct) and yearly average. The increasing then declining phase are visible for all of this time strata. Interestingly, the bigeye standardized CPUE present at this Working Party (Matsumoto et al, 2016) exhibits an overall declining trend as the shear increases, and increasing trend as the shear gets weaker. There are many factors to consider in CPUE standardization but incorporation of vertical shear indices could be recommended for further analyses.

Acknowledgements

We are grateful to the Climate Centre of the Seychelles National Meteorological Services, and particularly to Marcel Belmont, a senior technician of this Centre, for the provision of sea level pressure data used in this paper.

References

- Aaron, F., Levine, Z. & McPhaden, M.J. (2016). How the July 2014 easterly wind burst gave the 2015-2016 El Niño a head start. *Geophys. Res. Letters*, 43(12): 6503-6510
- Boggs, C.H. (1992) Depth, capture time, and hooked longevity of longline-caught pelagic fish: timing bites of fish with chips. *Fish. Bull. U.S.* 90:642–658
- Huang, B., V.F. Banzon, E. Freeman, J. Lawrimore, W. Liu, T.C. Peterson, T.M. Smith, P.W. Thorne, S.D. Woodruff, and H.-M. Zhang (2015). Extended Reconstructed Sea Surface Temperature version 4 (ERSST.v4): Part I. Upgrades and intercomparisons. *Journal of Climate*, doi:10.1175/JCLI-D-14-00006.1
- Marsac, F. (2011). Outline of climate and oceanographic conditions in the Indian Ocean : an update to August 2011. Oral presentation at the 13th session of the WPTT, IOTC. IOTC-2011-WPTT13-Rev1.
- Marsac, F. (2012). Outline of climate and oceanographic conditions in the Indian Ocean over the period 2002-2012. 14th session of the IOTC Working Party on Tropical Tunas, Mauritius, 24-29/10/2012. IOTC-2012-WPTT14-09, 16 p.

- Marsac, F (2013). Outline of climate and oceanographic conditions in the Indian Ocean; an update to August 2013. 15th Session of the Working Party on Tropical Tuna. IOTC-2013-WPTT15-09, 14 p
- Marsac, F (2014). Outline of climate and oceanographic conditions in the Indian Ocean; an update to August 2014. 16th Session of the Working Party on Tropical Tuna. IOTC-2014-WPTT16-24, 15 p
- Marsac, F. (2015). Outline of climate and oceanographic conditions in the Indian Ocean; an update to August 2015. 16th Session of the Working Party on Tropical Tuna. IOTC-2015-WPTT17-09, 16 p
- Marsac, F., Le Blanc, J-L. (1998). Interannual and ENSO-associated variability of the coupled ocean-atmosphere system with possible impacts on the yellowfin tuna fisheries of the Indian and Atlantic oceans. In: J.S. Beckett (Ed). ICCAT Tuna Symposium. *Coll. Vol. Sci. Pap.*, L(1) : 345-377.
- Matsumoto, T., Nishida, T., Satoh, K., Kitakado, T. (2016). Japanese longline CPUE for bigeye tuna in the Indian Ocean standardized by GLM. IOTC-2016-WPTT18-13. IOTC Working Party on tropical Tunas, Seychelles, 5-10 Nov 2016.
- Saji, N.H., Goswami, B.N., Vinayachandran, P.N., Yamagata, T. (1999). A dipole mode in the tropical Indian Ocean. *Nature* 401: 360-363
- Smith, T.M., Reynolds, R.W., Peterson, T.C., Lawrimore, J. (2008). Improvements to NOAA's Historical Merged Land-Ocean Surface Temperature Analysis (1880-2006). *J. Climate*, **2**: 2283-2296
- Webster, P. J., A. M. Moore, Loschnigg, J.P., Leben, R. R. (1999). Coupled oceanic-atmospheric dynamics in the Indian Ocean during 1997-98. *Nature*, **401**, 356-360.
-

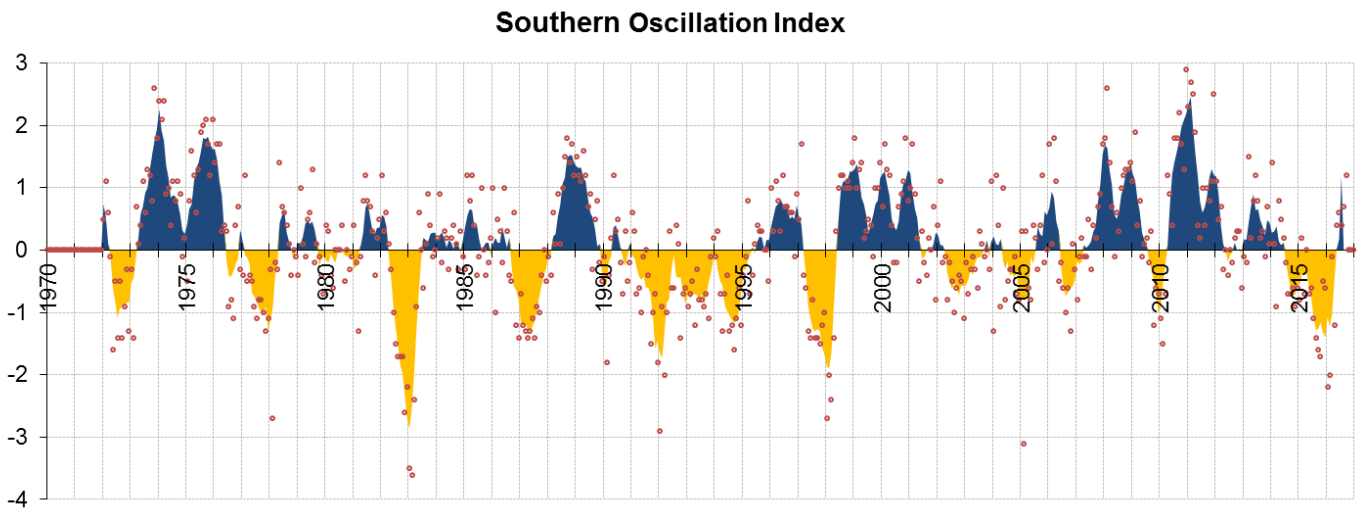


Fig.1 – The Southern Oscillation Index (SOI), January 1970 to September 2016. The color shaded area represents the 5-month moving average, whereas observed monthly values are shown in red dots. El Niño events correspond to the extreme negative values whereas La Niña events are described by the extreme positive values

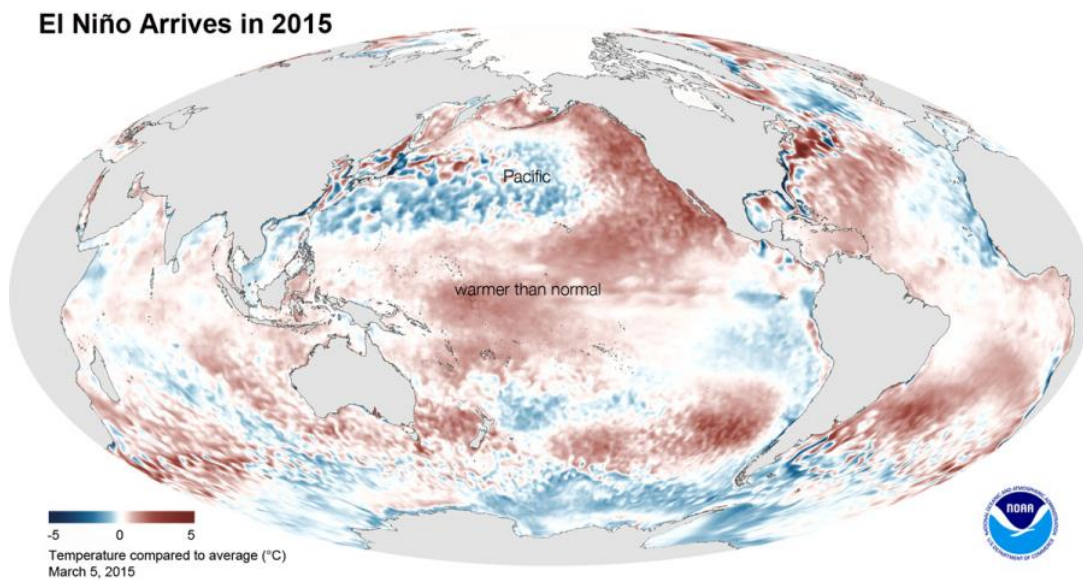


Fig.2 – SST anomalies in the Pacific Ocean on 5 March 2015. The large area of warm water in the central Pacific was induced by the aborted El Niño conditions of spring 2014 (source: NASA)

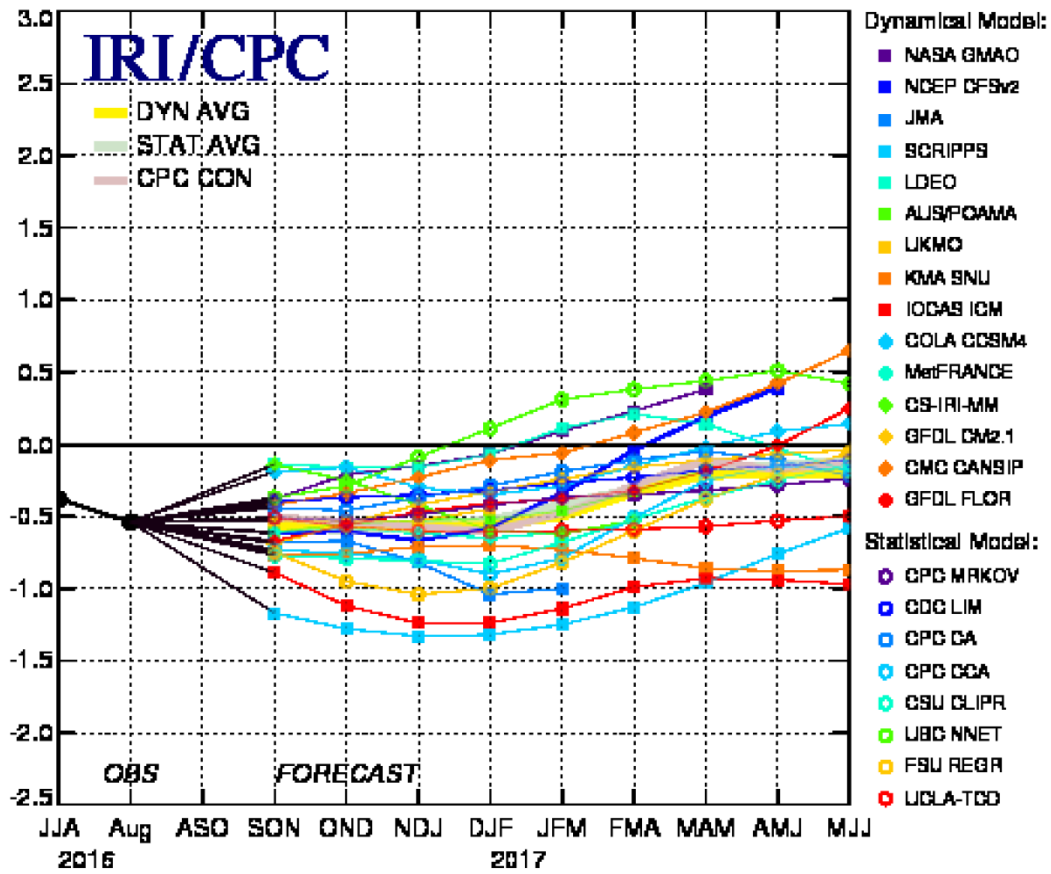


Fig.3 – Mid-September 2016 plume of Model ENSO predictions
 (Source : Climate Diagnostic Bulletin, Sept 2016, NOAA)

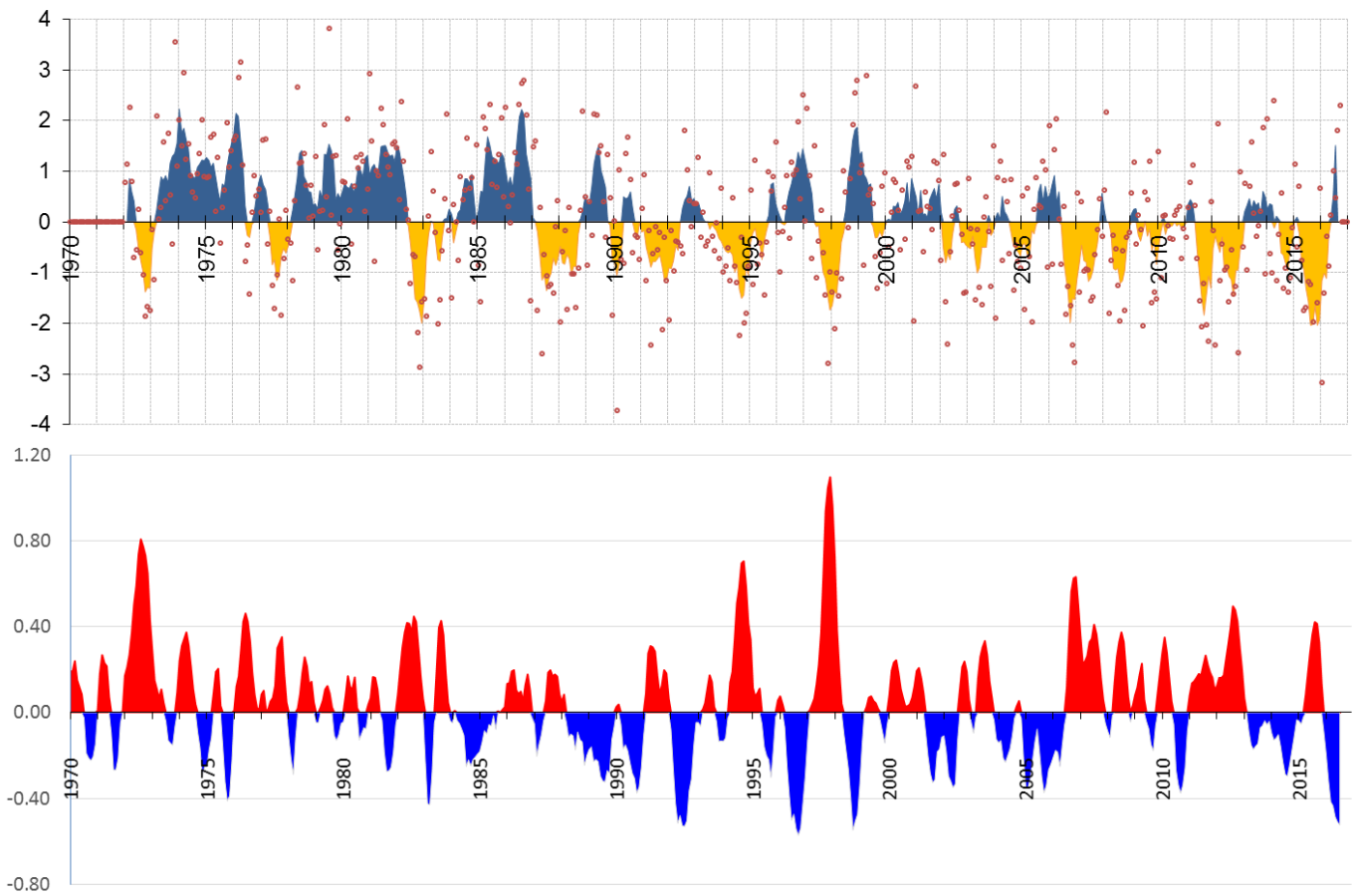


Fig. 4 - Indian Oscillation Index (top) and dipole mode index (bottom) over the period January 1970 – Sept 2016. The shaded area of IOI is a 5-months moving average whereas observed monthly values are represented in red dots. The DMI series is 5-month moving average. Warm (cold) events are represented by negative (positive) IOI and positive (negative) DMI. For a given anomaly, IOI and DMI are opposite sign.

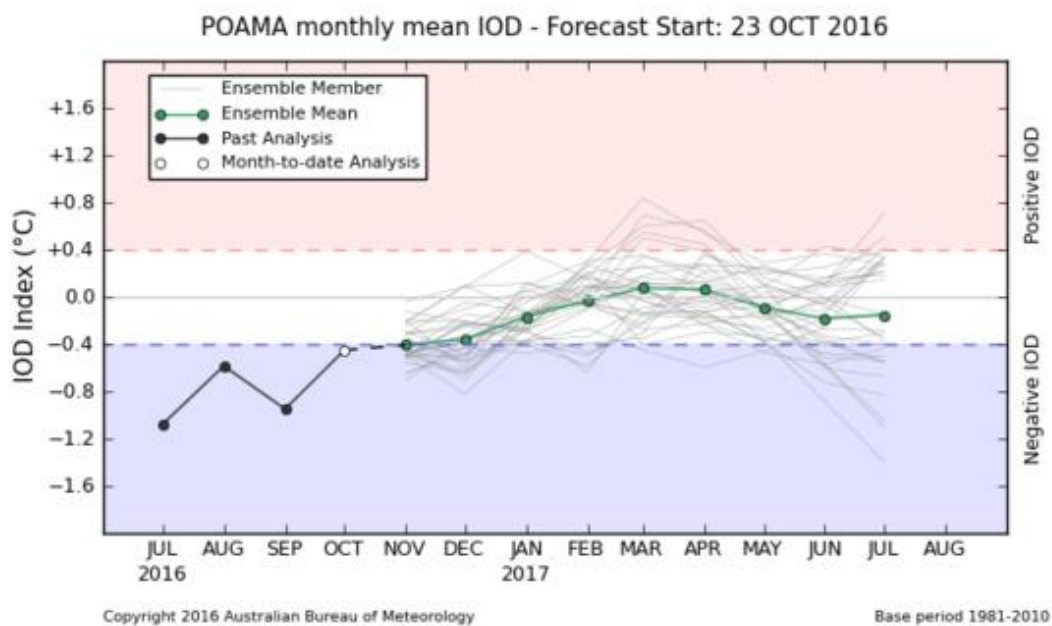


Fig. 5 - Indian Ocean Dipole forecast analysis (Australian Bureau of Meteorology)

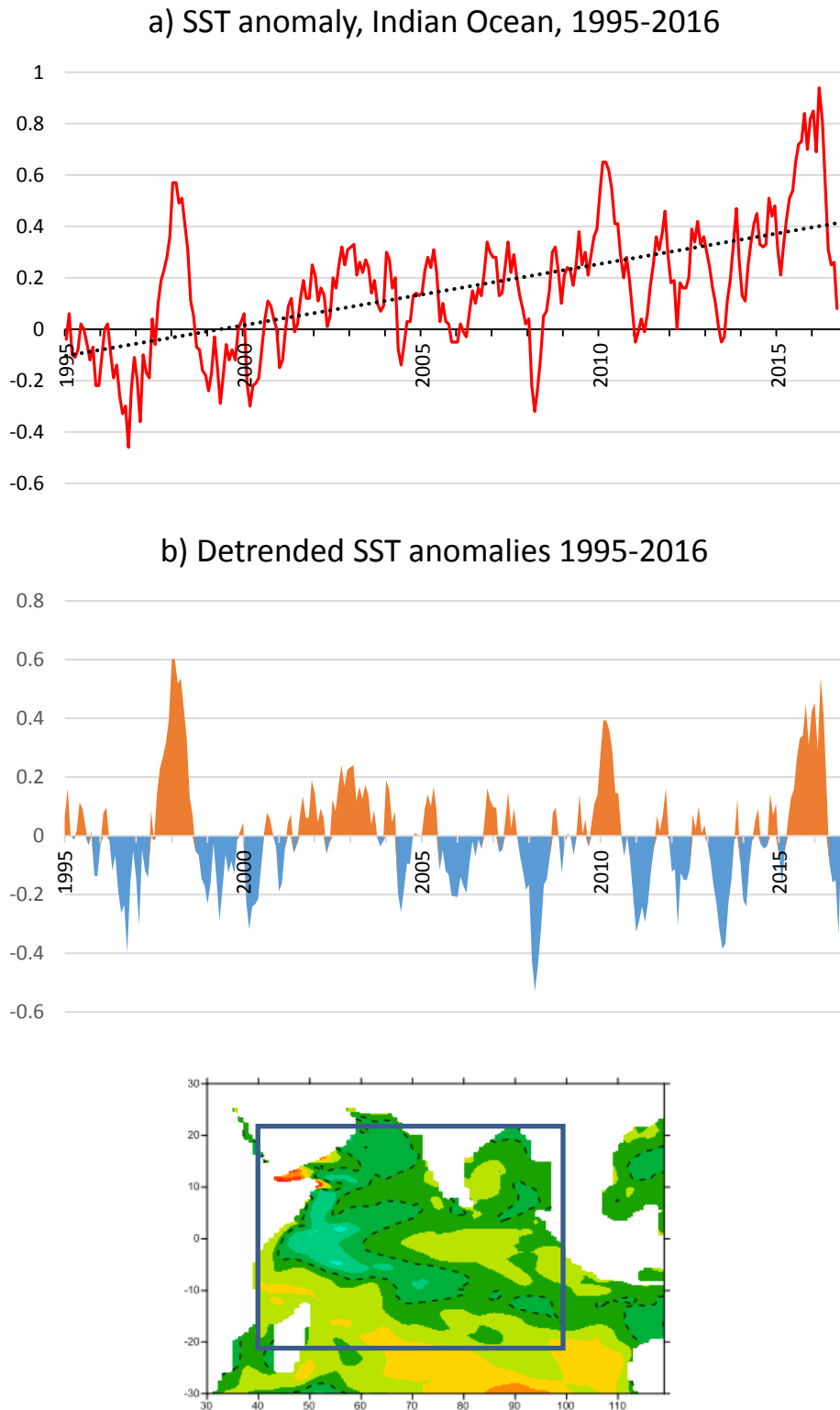


Fig. 6 – SST anomalies in the Indian Ocean measured from the ERSST v4 data set (Smith et al, 2008). a) monthly series Jan 1995-Jul 2016; b) detrended monthly series. The square in the map indicates the limits of the area considered.

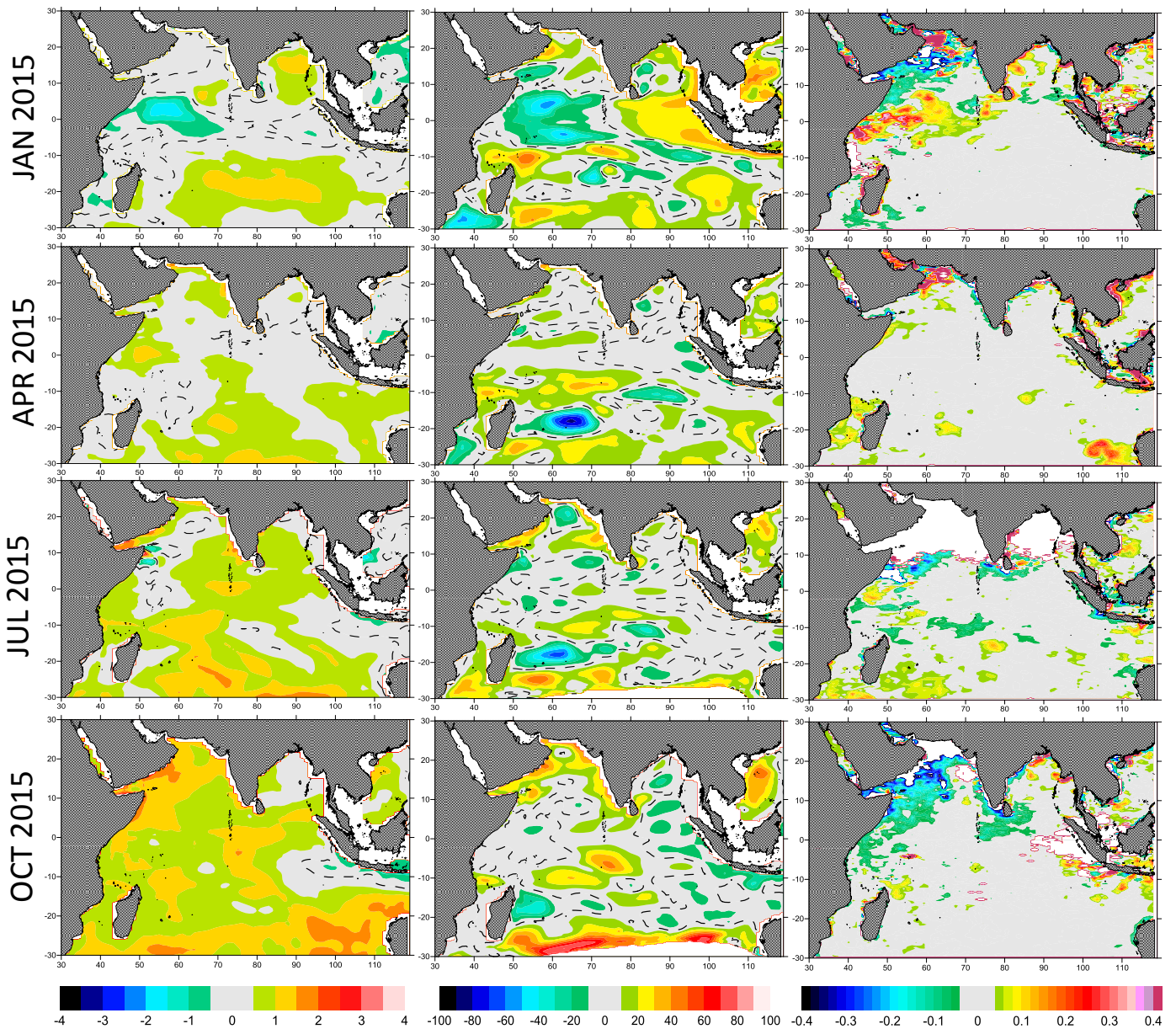


Fig. 7a – Geographic distribution of anomalies for sea surface temperature (°C, left), 20°C isothermal depth (m, middle) and sea surface chlorophyll (mg.m⁻³, right) in 2015. Grey shading indicates minor anomalies about the mean. It allows to highlight the more significant anomalies (colour shading).

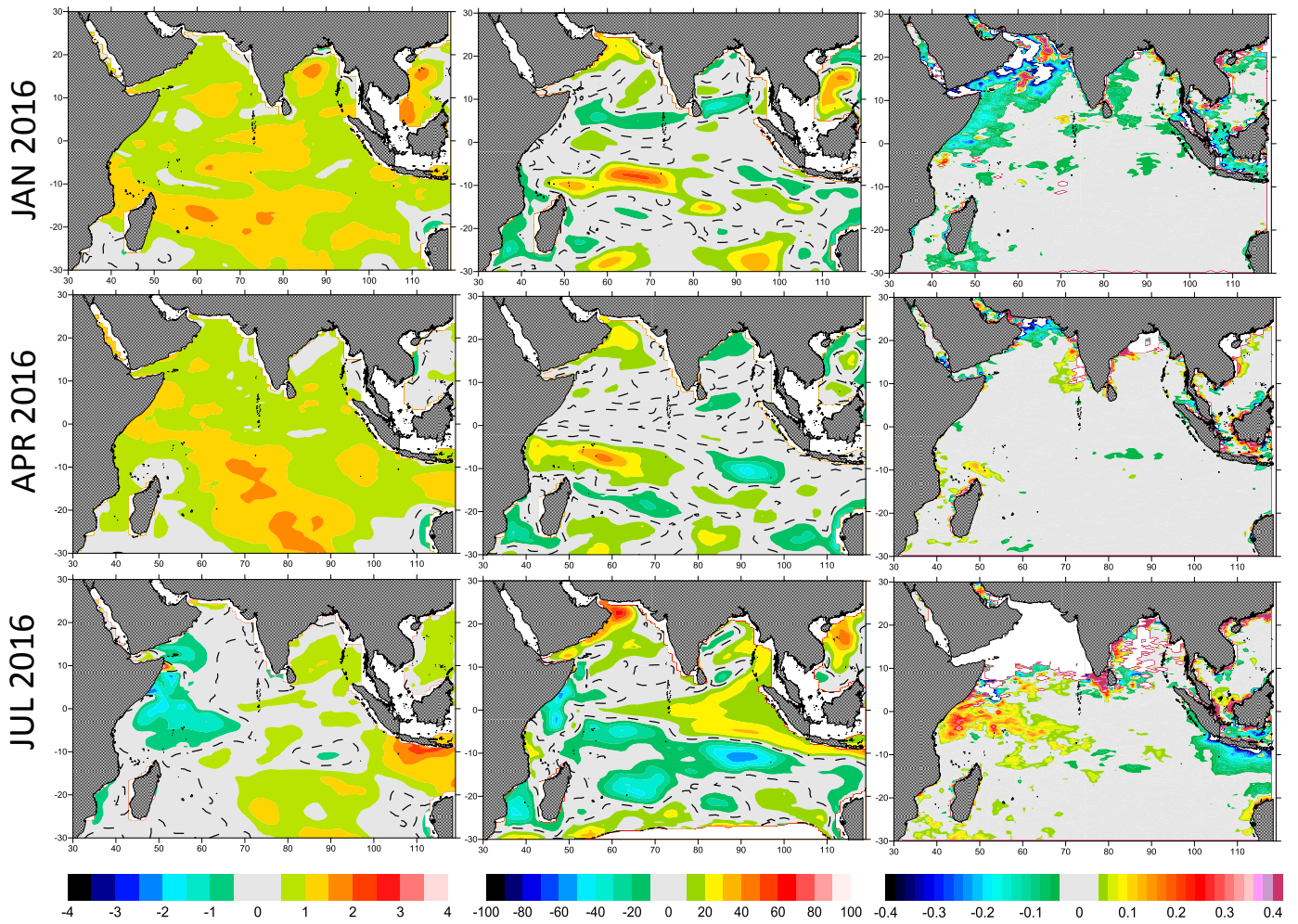


Fig. 7b – Geographic distribution of anomalies for sea surface temperature (°C, left), 20°C isothermal depth (m, middle) and sea surface chlorophyll (mg.m⁻³, right) in 2016. Grey shading indicates minor anomalies about the mean. It allows to highlight the more significant anomalies (colour shading).

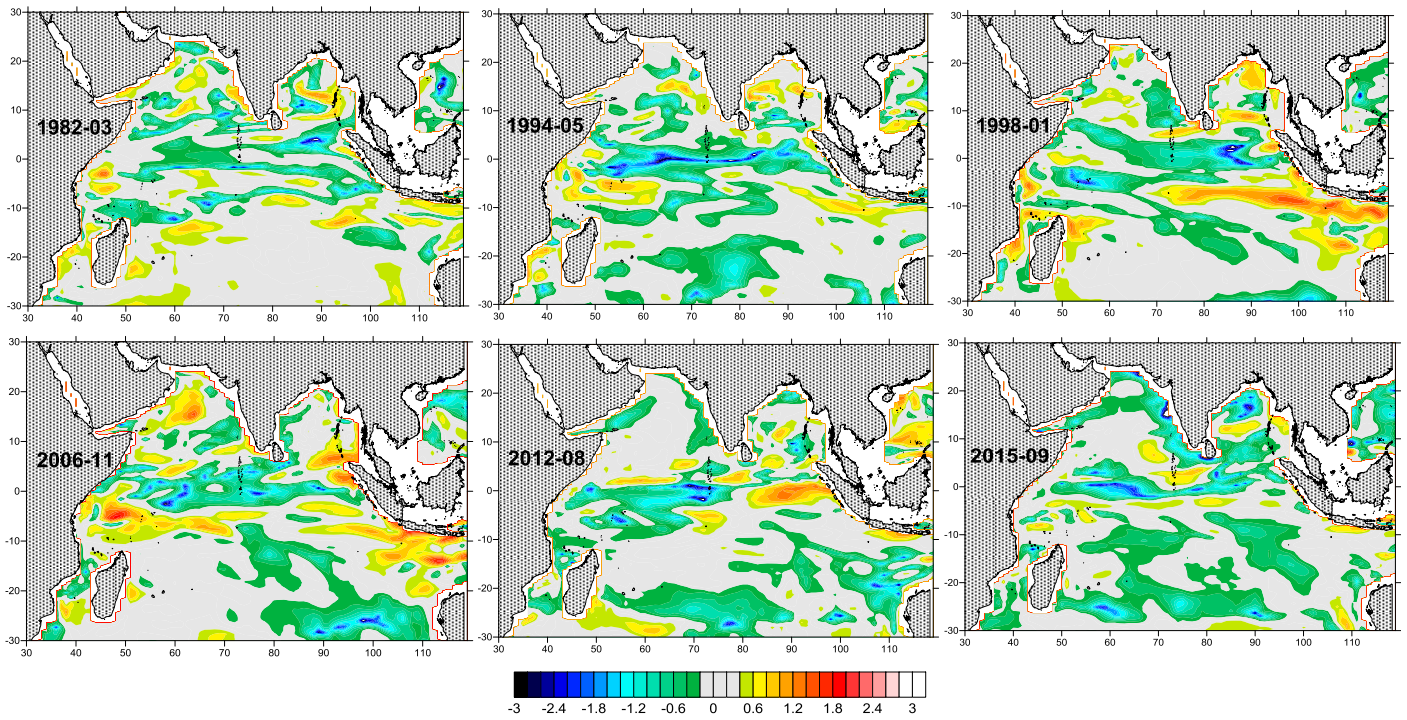


Fig.8 – Geographic distribution of the vertical current shear (between 5 and 145m) during positive dipole events

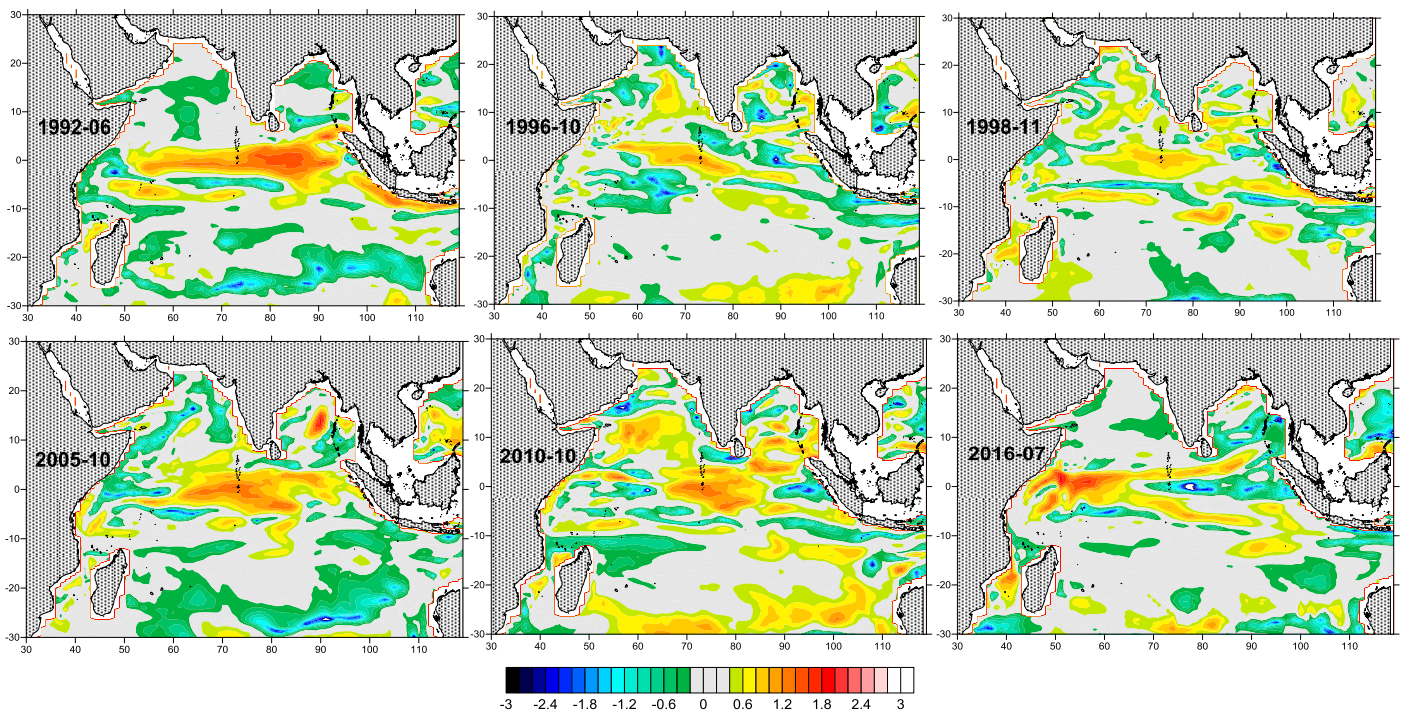


Fig.9 – Geographic distribution of the vertical current shear (between 5 and 145m) during negative dipole events

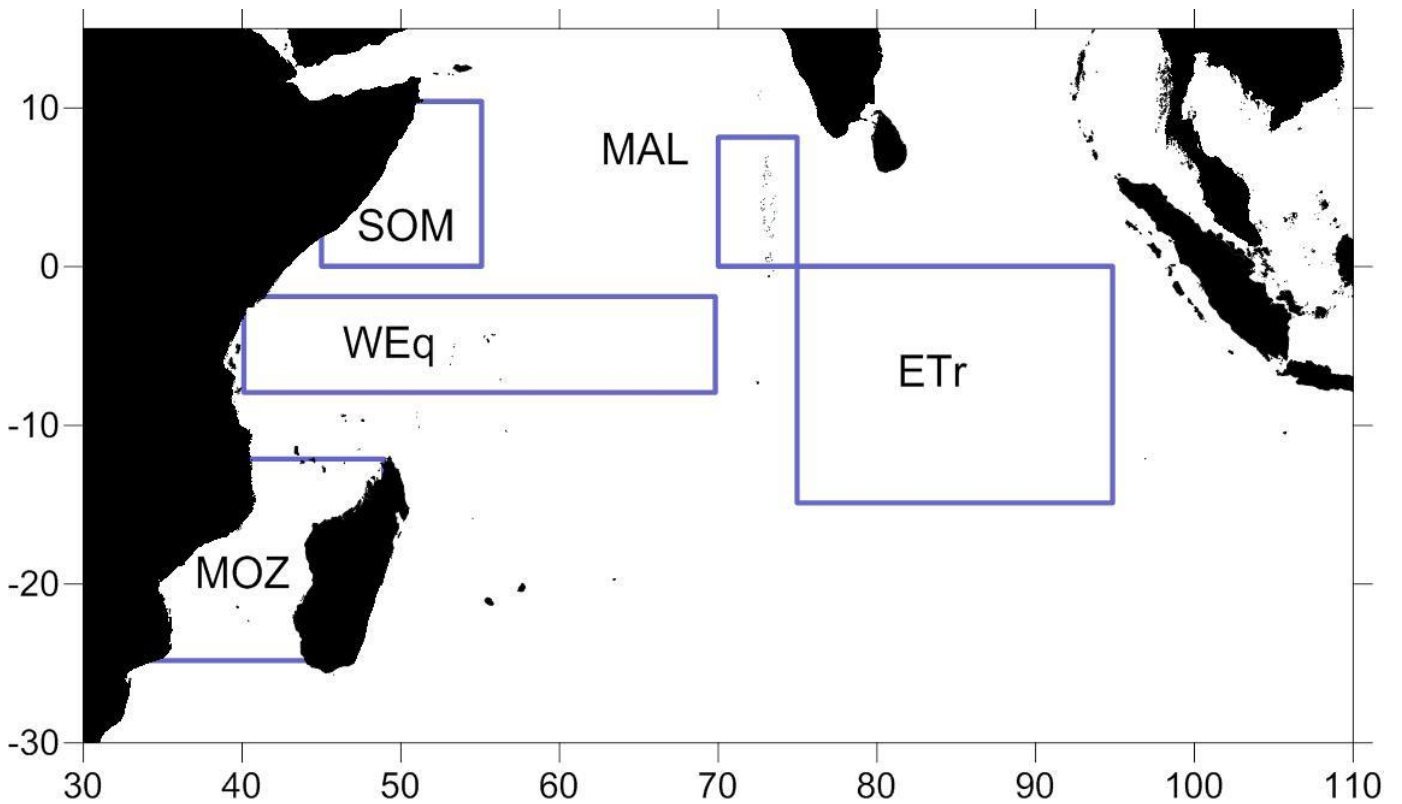


Fig. 10 - Area stratification used for the regional analysis.

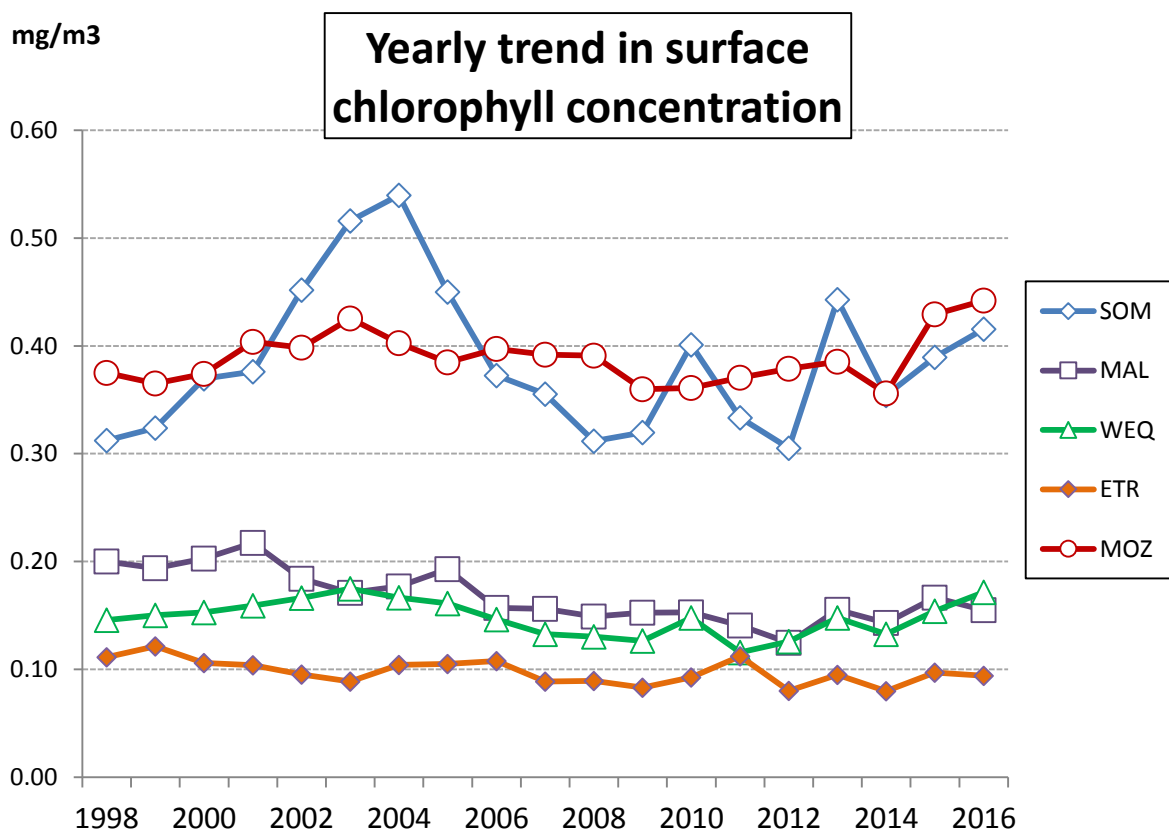


Fig.11 – Yearly trend of sea surface chlorophyll concentration measured by satellite, 1998-2016 (Seawifs 1998-2002 / Modis since 2003). Note that 2016 is incomplete (ends in September).

SOMALIA

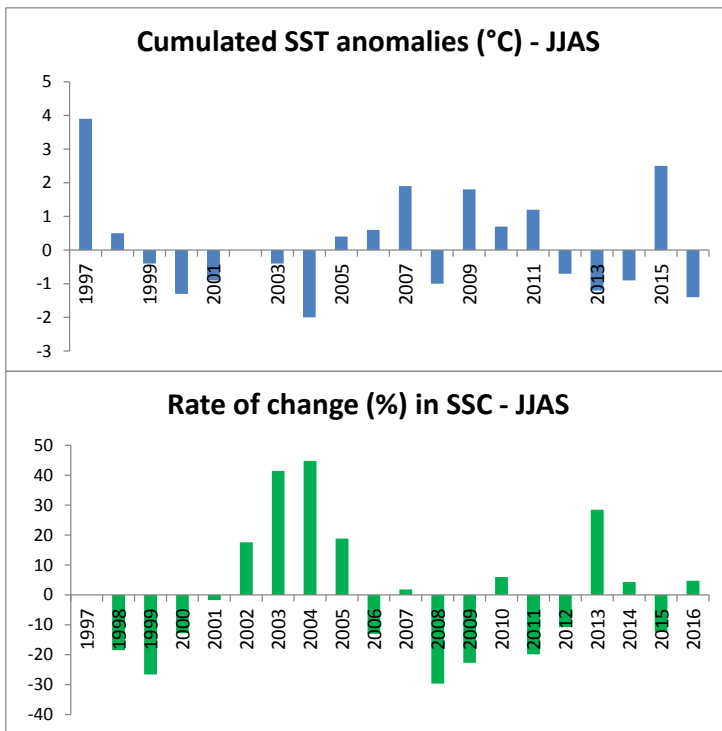


Fig. 12 – SST and surface chlorophyll (SSC) trends during the south-west monsoon, average June to September, in the Somalian basin. SST anomalies are cumulated over the season. Chlorophyll is expressed as rate of change about the 1998-2016 mean, June to September.

MOZAMBIQUE CHANNEL

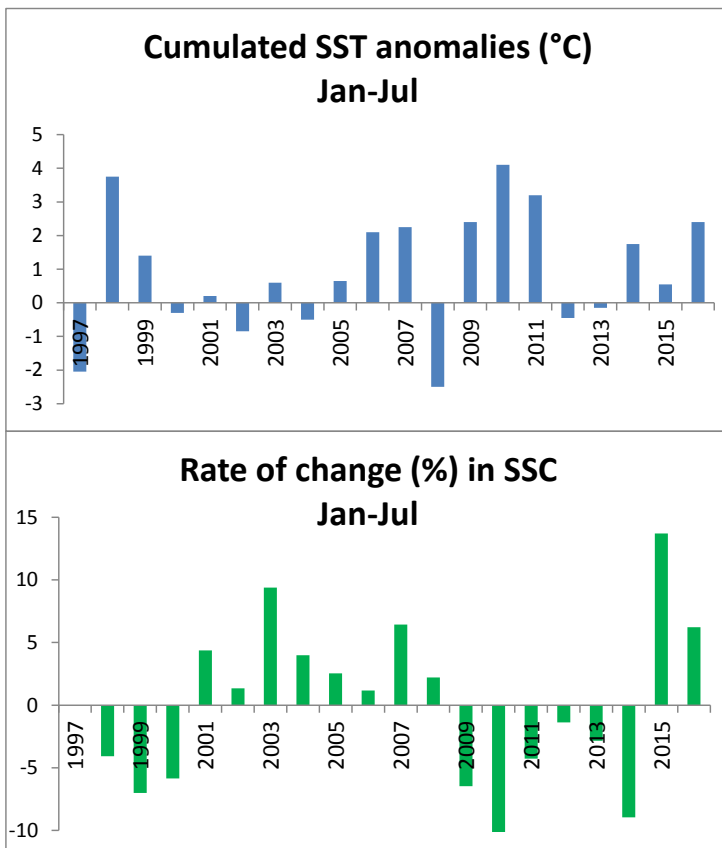


Fig. 13 – SST and surface chlorophyll (SSC) trends in the Mozambique Channel. Statistics are calculated for the period January to August. SST anomalies are cumulated over the period and chlorophyll is expressed as rate of change about the 1998-2016 mean for the study period.

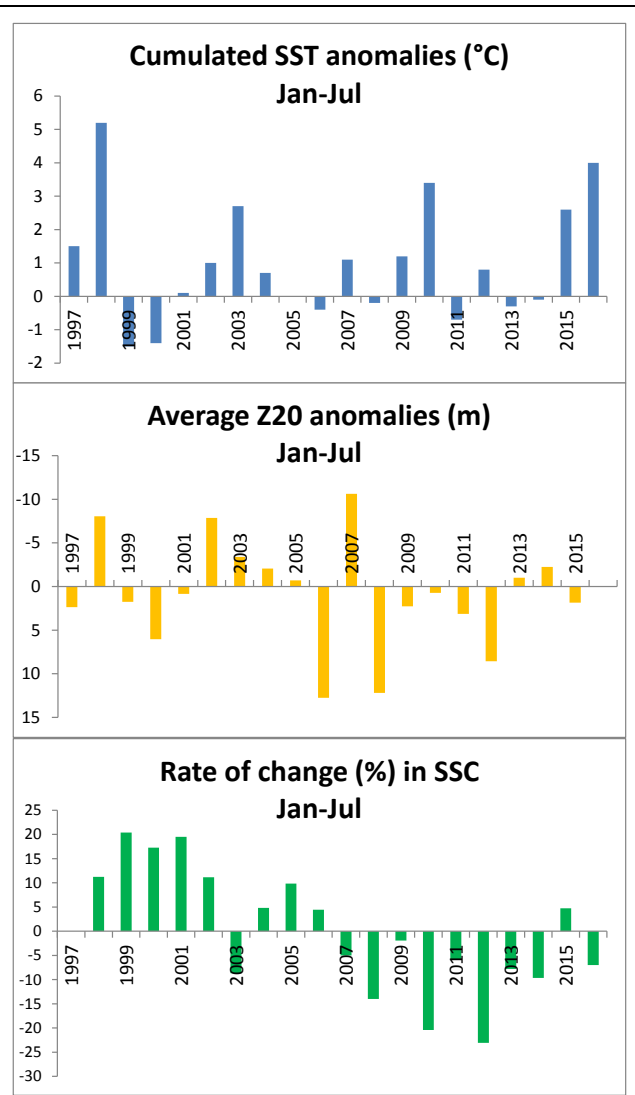
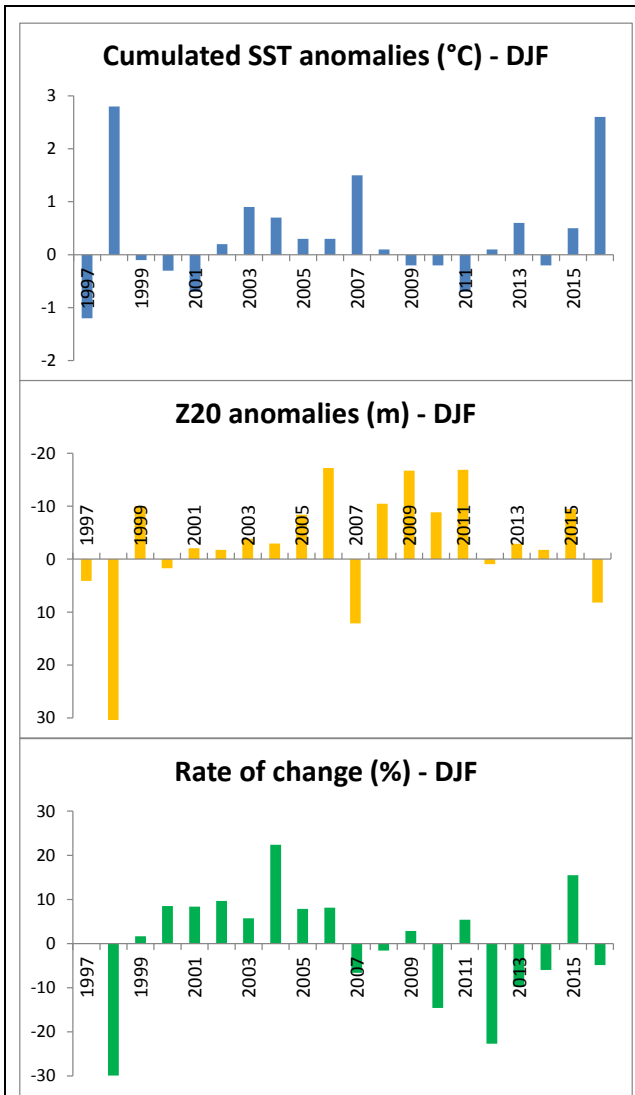
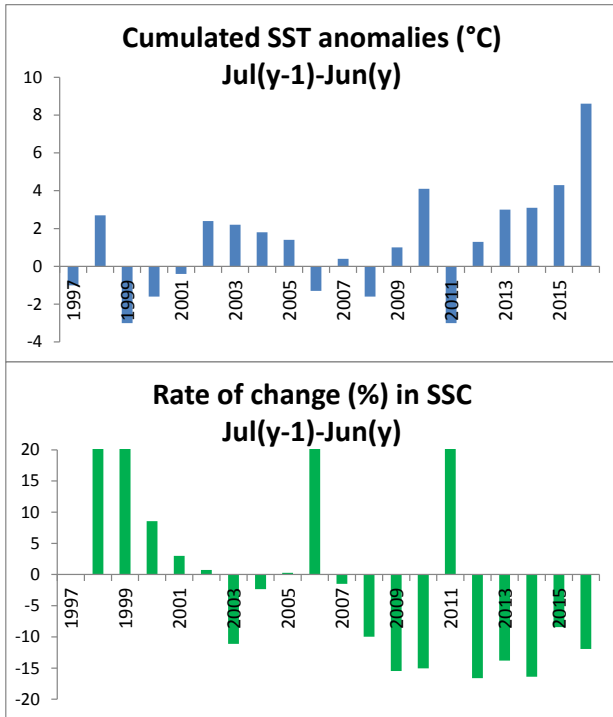


Fig. 14 – SST, 20°C isothermal depth and surface chlorophyll trends in the West Equatorial area, during the core of the north-east monsoon (December to February). SST anomalies are cumulated over the season, MLD anomalies are the mean over the season and chlorophyll is expressed as rate of change about the 1998-2016 average for the season. Negative (positive) MLD anomalies denote shoaling (deepening) of the thermocline.

WEST EQUATORIAL AREA

Fig. 15 – SST, MLD and surface chlorophyll (SSC) trends in the Maldives. Statistics are calculated for the period January to July. SST anomalies are cumulated over the period, MLD anomalies are the average over the period and chlorophyll is expressed as rate of change about the 1998-2016 for the study period. Negative (positive) MLD anomalies denote shoaling (deepening) of the thermocline.

MALDIVES



EAST TROPICAL AREA

Fig. 16 – SST and chlorophyll (SSC) trends in the Eastern Tropical Indian Ocean, 12-month average from July (of the preceding year) to June (of the current year). SST anomalies are cumulated over the 12-month period and SSC is expressed as rate of change about the 1998-2016 for the same period.

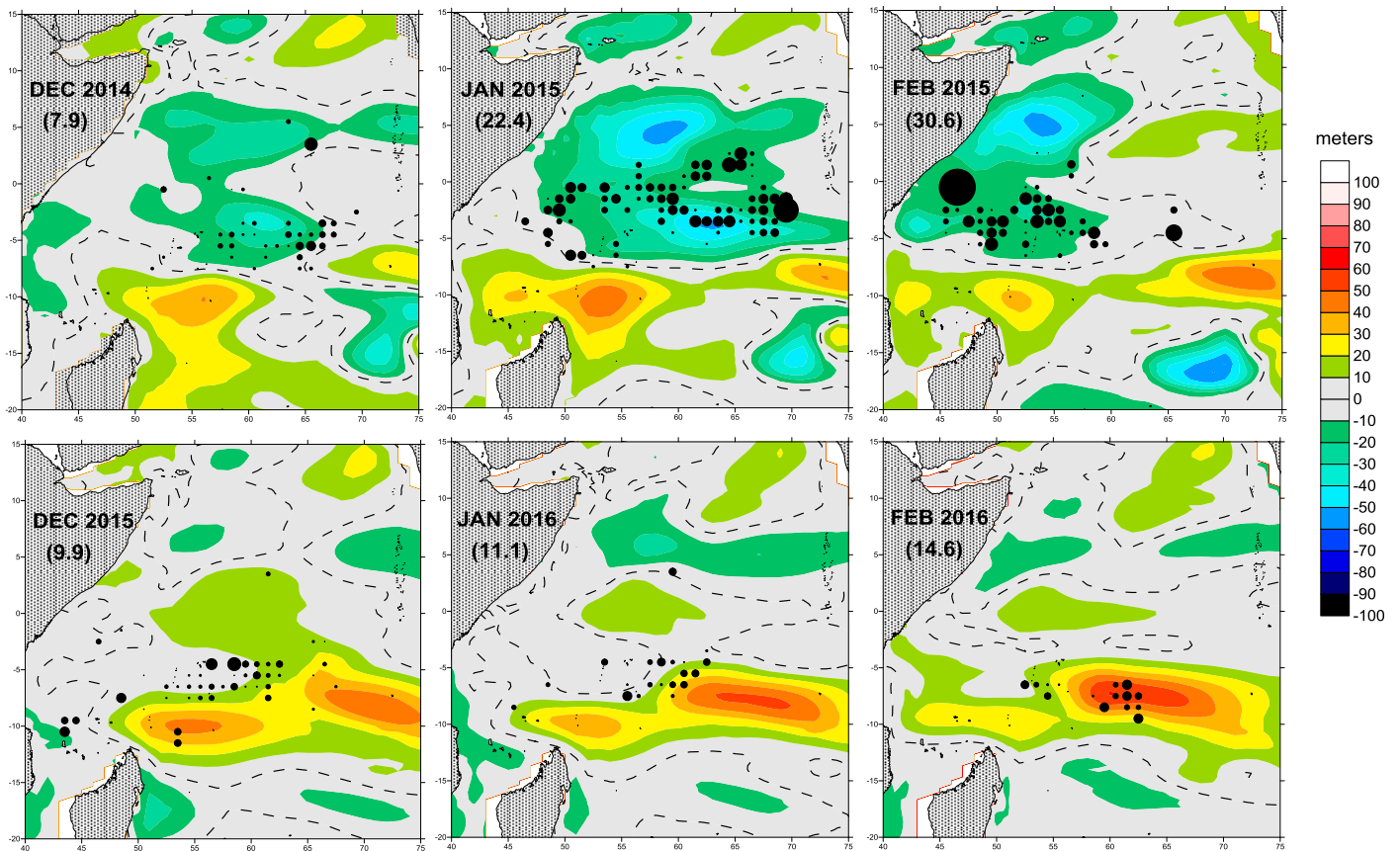


Fig.17 – Distribution of yellowfin purse seine CPUEs on free schools during two fishing seasons (black circles) and corresponding thermocline depth anomalies (color shade with scale on the right, in meters). Number in brackets in the legend indicates the average CPUE for the month (in tons/fishing day). Top: Dec 2014-Feb 2015. Bottom: Dec 2015-Feb 2016.

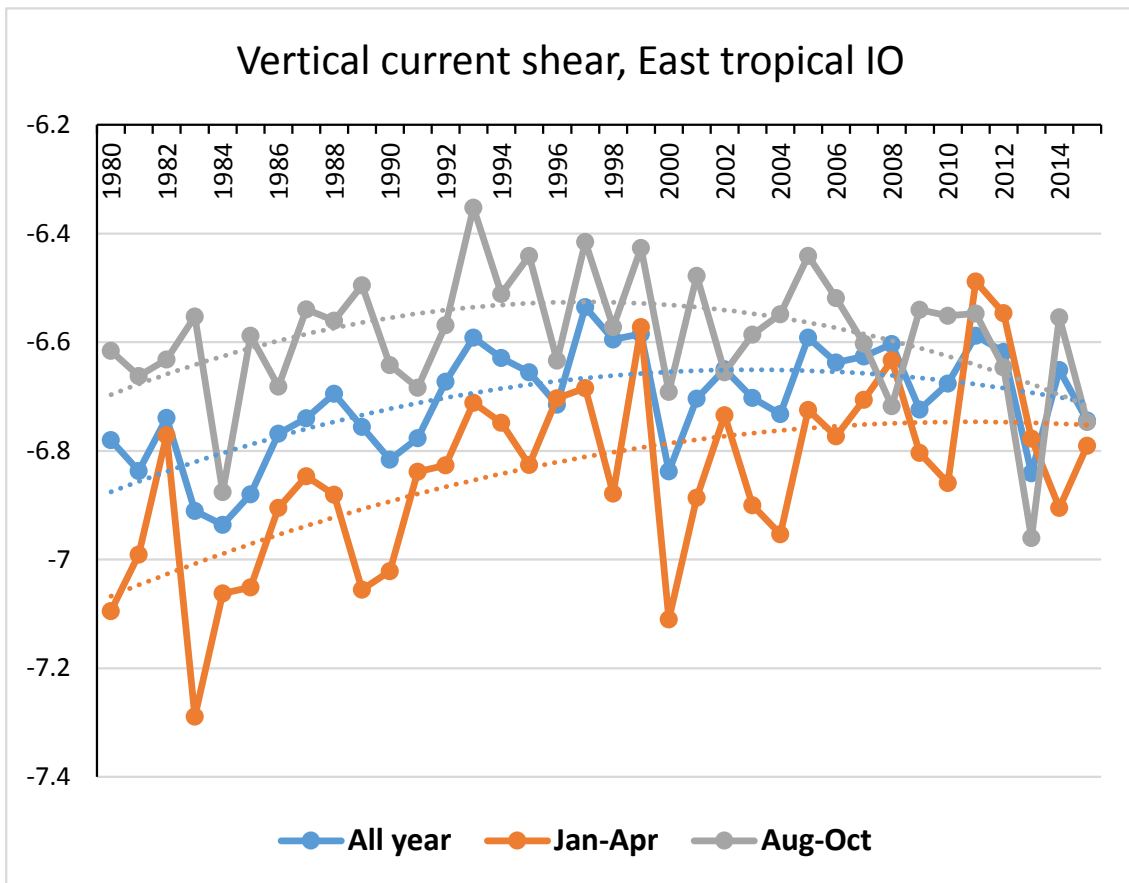


Fig.18 – Time series and long-term trend of the vertical current shear between 5m and 145m, for 1980-2015. Note the shear is expressed in a log scale. The selected area correspond to the Japanese longline core fishing zone for bigeye (80°E-100°E / 0°-15°S). Series are given for the season of low shear (Jan-April), high shear (Aug-Oct) and the yearly average.